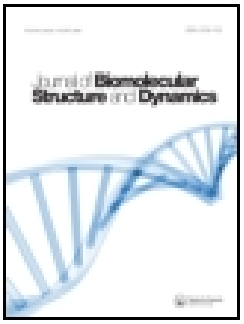

Taylor & Francis
Taylor & Francis Group

Journal of Biomolecular Structure and Dynamics

ISSN: (Print) (Online) Journal homepage: https://www.tandfonline.com/loi/tbsd20

Unassisted N-acetyl-phenylalanine-amide transport across membrane with varying lipid size and composition: kinetic measurements and atomistic molecular dynamics simulation

Brent L. Lee , Krzysztof Kuczera , Kyung-Hoon Lee , Ed W. Childs & Gouri S. Jas

To cite this article: Brent L. Lee , Krzysztof Kuczera , Kyung-Hoon Lee , Ed W. Childs & Gouri S. Jas (2020): Unassisted N-acetyl-phenylalanine-amide transport across membrane with varying lipid size and composition: kinetic measurements and atomistic molecular dynamics simulation, Journal of Biomolecular Structure and Dynamics, DOI: 10.1080/07391102.2020.1827037

To link to this article: https://doi.org/10.1080/07391102.2020.1827037

JOURNAL OF BIOMOLECULAR STRUCTURE AND DYNAMICS
https://doi.org/10.1080/07391102.2020.1827037

Unassisted N-acetyl-phenylalanine-amide transport across membrane with varying lipid size and composition: kinetic measurements and atomistic molecular dynamics simulation

Brent L. Lee[a], Krzysztof Kuczera[a,b], Kyung-Hoon Lee[c], Ed W. Childs[d] and Gouri S. Jas[e]

[a]Department of Chemistry, The University of Kansas, Lawrence, KS, USA; [b]Department of Molecular Biosciences, The University of Kansas, Lawrence, KS, USA; [c]Department of Biology, Chowan University, Murfreesboro, NC, USA; [d]Department of Surgery, Morehouse School of Medicine, Atlanta, GA, USA; [e]Department of Pharmaceutical Chemistry, The University of Kansas, Lawrence, KS, USA

Communicated by Ramaswamy H. Sarma

ABSTRACT

Biological membranes are essential to preserve structural integrity and regulate functional properties through the permeability of nutrients, pharmaceutical drugs, and neurotransmitters of a living cell. The movement of acetylated and amidated phenylalanine (NAFA) across 1,2-dioleoyl-sn-glycero-3-phosphocholine (DOPC) and 1-palmitoyl-2-oleoyl-*sn*-glycero-3-phosphocholine (POPC) membrane bilayers is investigated to probe physical transport. The rate of transport is measured experimentally applying parallel artificial membrane permeation assay (PAMPA). At the physiological temperature, 310 K, the measured time constants in the neutral pH were ~6 h in DOPC and ~3 h in POPC, while in a more acidic condition, at a pH 4.8, the time constants were ~8 h in both lipids. Computationally, we have expanded our transport study of three aromatic dipeptides across a bilayer composed of DOPC[18]. In this study, we have examined the effects of lipid composition and bilayer size on the passive transport of NAFA by simulating the dipeptide in three different bilayers, with 50 DOPC lipids, 50 POPC lipids, and 40 POPC molecules. Specifically, atomistic molecular dynamics simulations with umbrella sampling were used to calculate the potential of mean force for the passive permeation of NAFA across the bilayers. Diffusion constants were then calculated by numerically solving the Smoluchowski equation. Permeability coefficients and mean first passage times were then calculated. Structural properties – Ramachandran plots, sidechain torsions, peptide insertion angles, radial distribution functions, and proximal peptide water molecules – were also examined to determine the effect of system size and lipid type. In terms of systems size, we observed a small decrease in the highest barrier of the potential of mean force and fewer sampled sidechain dihedral angle conformations with 40 versus 50 POPC lipids due to weaker membrane deformations within a smaller lipid bilayer. In terms of lipid type, DOPC contains two monounsaturated acyl chains compared to only one such acyl chain in POPC; therefore, DOPC bilayers are less ordered and more easily deformed, as seen by a much broader potential of mean force profile. The NAFA in DOPC lipid also transitioned to an internally hydrogen-bonded backbone conformation at lower membrane depths than in POPC. Similarly, as for other aromatic dipeptides, NAFA tends to insert into the membrane sidechain-first, remains mostly desolvated in the membrane center, and exhibits slow reorientations within the bilayer in both DOPC and POPC. With a joint experimental and computational study we have gained a new insight into the rate of transport and the underlying microscopic mechanism in different lipid bilayer conditions of the simplest hydrophobic aromatic dipeptide.

ARTICLE HISTORY
Received 24 July 2020
Accepted 17 September 2020

KEYWORDS
Unassisted transport; aromatic dipeptide; lipid bilayer; transport kinetics; DOPC; POPC; molecular dynamics simulation

Introduction

One of the most fundamental physicochemical properties of biological membranes is to preserve cellular structural integrity and regulate functional property through the permeability of nutrients, pharmaceutical drugs, and neurotransmitters. It is suggested that the permeability across membrane lipid bilayer occurs most commonly by a passive diffusion process at a rate associated with the lipophilicity of the permeant (Dobson et al., 2009; Dobson & Kell, 2008; Giacomini et al., 2010; Hogben et al., 1959; Högerle & Winne, 1983). Transport across the biological membrane is an integral component in the study of pharmacokinetics. Though passive diffusion is thought to be the dominant pathway for transport across the lipid bilayer, many transporter proteins have been identified as facilitators for drug transport (Cohen & Bangham, 1972; Corti et al., 2006; Fredriksson et al., 2008; Irvine et al., 1999; Meier et al., 2006; Seelig, 2007; Xiang & Anderson, 1998; Zhu et al., 2002). To screen for membrane permeability of bioactive compounds several assays have been developed, with one commonly used in the pharmaceutical industry and in academia being parallel artificial membrane permeability (PAMPA) (Cardenas et al., 2012; Di et al., 2003; Kansy et al.,

CONTACT Gouri S. Jas gouri.jas@physicianscientists.org Department of Pharmaceutical Chemistry, The University of Kansas, Lawrence, Kansas 66047, USA
Supplemental data for this article can be accessed online at https://doi.org/10.1080/07391102.2020.1827037.

1998; Lee et al., 2016; Wohnsland & Faller, 2001). PAMPA assay characterizes the passive diffusion of permeant through macroscopically flat synthetic membranes with the composition that has been optimized to model the permeability across a phospholipid bilayer. Investigation of permeability of the aromatic molecules across lipid bilayers is of significant interest as aromatic moieties are ubiquitously present in biologically important molecules such as proteins, peptides, hormones, neurotransmitters as well as pharmaceutics. Fluorescently labeled permeants have been employed to study membrane transport which can substantially complicate the understanding of fundamental permeability characteristics. This may be a reason for the fascination of a label-free fluorescence-based transport assays.

The kinetic profile of a permeant under a specific bilayer environment can be obtained with PAMPA assays and be directly associated with categorizing the membrane permeation behavior of different analytes (Cardenas et al., 2012; Lee et al., 2016). The characteristics documented from these experimental measurements and analysis can provide a roadmap for testing the drug candidates. The kinetic screening experiments can methodically divide permeants into fast, slow, and non-permeating agents. Molecular dynamics (MD) simulations can, in principle, provide an atomically detailed description of permeation through membrane bilayer. It has become an essential tool to study permeation since the work of Marrink and Berendsen (1994). There are essentially two proposed approaches to study permeation in the absence of a facilitator. In one scenario the permeant moves across a transient water pore and the other is where it directly permeates through the membrane bilayer. The simulation approach with direct permeation across bilayer is applied in the current investigation. Even though the classification of permeability is critically important in the field of drug discovery, there is little knowledge about the influence of bilayer composition and size on the permeating agent. It has been suggested that lipids with longer chain length exhibit a slower rotational motion with a broader free energy profiles and statistically unaltered local diffusion constants (Klauda et al., 2008). The study with paracetamol in an unsaturated lipid bilayer composed of linear acyl chains with 14 and 16 carbon atoms found no effect on the free energy profile and hydrogen bonding between paracetamol and water with respect to these two chain lengths (Faulkner et al., 2020). The effect of permeation due to lipid size with varying number of lipid molecules and a charged arginine found a reduction in the free energy barrier of the larger system with substantial deformation (Shinoda, 2016). Considerable effort is devoted to exploring the microscopic mechanism of molecular transport across membrane bilayer under passive condition (Bassolino-Klimas et al., 1993; 1995; Snyder et al., 2002; Tu et al., 1996; Vaz & Almeida, 1991; Venable et al., 2000; Xiang & Anderson, 2006). Direct MD simulations to understand solute diffusivity in model lipid bilayers were investigated (Bassolino-Klimas et al., 1993; 1995). How molecular transport through lipid bilayer is influenced by the lipid composition and the system size is not clearly understood. Efforts have been made to understand the effects of lipid type and model system size on the permeation process (Awoonor-Williams & Rowley, 2016; Lee & Kuczera, 2018; Marrink & Berendsen, 1996). Permeation study with small molecules like H_20, O_2, CO, and NO through lipid bilayers with unsaturated, linear acyl chains of carbon length with 12-C, 14-C, and 16-C (Sugii et al., 2005) suggested that lipids undergo slower rotational motion and demonstrate larger and broader free energy profiles. The effect of system size on the permeation of small molecules with different numbers of lipid molecules per bilayer with linear unsaturated tails showed that the free energy barrier in the larger system was lowest (Bonhenry et al., 2013; Hu et al., 2013; Nitschke et al., 2016).

We have described, earlier (Cardenas et al., 2012; Lee et al., 2016), the passive permeation of three aromatic aminoamides in zwitterionic and in neutral (tryptophan, NATA, tyrosine, NAYA, and phenylalanine, NAFA) condition across DOPC bilayers. Measured transport times were found to be between 5 and 10 hr for NATA, NAYA, and NAFA where the rate of translocation for NAFA was the fastest and NAYA the slowest. At a lower pH the transport rate for NAYA and NATA was faster and the NAFA, slower. Computationally, applying umbrella sampling simulations, we have calculated free energy profiles, diffusion constants, and permeabilities. The peptides tended to bind preferentially to the membrane surface and encounter a high free energy barrier in the membrane center. While the peptide translational diffusion rates tended to change little with depth of membrane insertion, the rotational diffusion in the bilayer was both very slow compared to solution and strongly position-dependent. Additionally, we found that the dipeptides favored the internally hydrogen-bonded backbone (C_{7eq}) conformation inside the membrane and tended to become desolvated in the central acyl chain region.

The primary goal of this work is to explore the effects of unassisted membrane transport of a dipeptide in different bilayer compositions employing experimental and computational studies. Additionally, computationally we set out to investigate the effects of the size and lipid type of involving bilayer model on the dipeptide permeation. Here, we apply joint experiments and atomistic MD simulations to better understand the permeation properties, rate of permeation, and the underlying mechanism with varying bilayer composition and the size employing a neutral aromatic amino acid, N-acetyl-phenylalanine-amide (NAFA). Experimentally, we have measured the kinetics of NAFA in two different lipid bilayers, consisting of DOPC and POPC phospholipids. The rate of transport is observed to be significantly different in POPC and DOPC under neutral pH. Whereas the measured rate of transport for NAFA across these two lipid bilayers, in the acidic environment, was found to be significantly slower. MD simulations with umbrella sampling are employed to describe the atomistic mechanism of the passive permeation of the phenylalanine dipeptide in three bilayer systems, consisting of 50 DOPC and 50 POPC and 40 DOPC lipids, respectively. Here DOPC contains acyl chains with 18 carbon atoms and one double bond near the

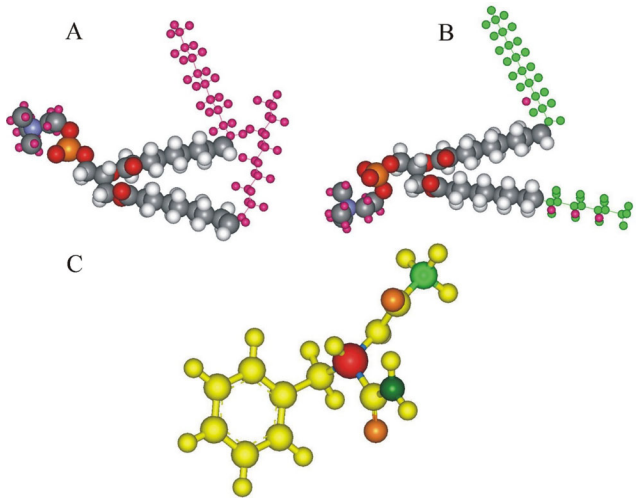

Figure 1. Molecules involved with this study are displayed. Figure 1(A) depicts DOPC and Figure 1(B) depicts POPC, with bends at the C = C bonds, and Figure 1(C) depicts the phenylalanine dipeptide.

center and POPC has two acyl chains, one acyl chain that is identical to DOPC and the other acyl chain with 16 carbons and no double bond. The three simulations were performed to examine the effect of bilayer composition and size on permeability characteristics, the potential of mean force, position-dependent diffusion constants, and the conformational dynamics of NAFA in DOPC and POPC.

Methods

Experimental

Material

DOPC (1,2-dioleoyl-sn-glycero-3-phosphocholine) and Egg yolk phosphatidylcholine (lecithin; L-α-phosphatidylcholine; POPC) were purchased from Avanti Polar Lipids (Alabaster, AL). Neutral amino acid with capped N and C termini, sodium acetate, sodium phosphate monobasic, sodium phosphate dibasic, phosphate-buffered saline tablets (P-4417), 1,9-decadiene (Aldrich 118303), cresyl blue, and lucifer yellow were purchased from Sigma (St. Louis, MO). Hydrophobic filter plates (PVDF membrane without underdrain; MAIPNTR10) and 96-well disposable transport receiver plates (MATRNPS50) were purchased from Millipore Corporation (Billerica, MA).

Experimental procedures

A detailed experimental procedure is published elsewhere (Cardenas et al., 2012; Lee et al., 2016). Briefly, the parallel artificial membrane permeation assay (PAMPA) was carried out to measure the unassisted permeation of N-acetyl-Phenylalanine-amide (NAFA). PAMPA has been widely used to study oral absorption, blood-brain barrier penetration, and skin permeation. NAFA was prepared at a concentration of 200 μM for all these measurements. Samples were prepared by dissolving the powdered form of NAFA in 20 mM sodium acetate buffer at pH 4.8 and 20-mM sodium phosphate buffer at pH 7.2. Lipid solutions for DOPC and POPC were prepared with 5% w/v in 1,9-decadiene. A very carefully controlled sonication was applied to POPC and DOPC to ensure complete dissolution. A 96-well receiver microplate (acceptor compartment) was filled with 280 μL of the corresponding buffer, and the PVDF filter plate (donor compartment) was fused on the buffer-filled acceptor plate. The measurements were carried out at a physiological temperature, at 310 K. The lipid solutions (5 μL) were carefully added onto the filter surface, avoiding pipet tip contact with the filter. Immediately after the corresponding amino acid samples (150 μL per each well) were applied to the lipid-bound filter plate. This protocol was repeated every 3 h, and the experiment was terminated at 30 h. The fluorescence intensity of the sample was monitored with a Fluorolog (Horiba Jobin Yvon Inc., Edison, NJ) with the excitation wavelength set to 260 nm for NAFA. Membrane integrity was tested with Lucifer yellow and Cresyl blue.

Molecular dynamics

The physical setup of our simulation systems followed a procedure similar to our earlier work (Lee et al., 2016). Briefly, initial coordinates for systems consisting of a blocked dipeptide. Ac-Phe-NH_2, or NAFA, lipid bilayer, water, and ions were generated using the Membrane Builder tool of CHARMM-GUI (Jo et al., 2007; 2009; Wu et al., 2014). The three systems are classified based on the type and number of lipids used as DOPC 50, POPC 50, and POPC 40, with DOPC denoting 1,3-dioleoyl-*sn*-glycero-3-phosphocholine and POPC 1-palmitoyl-2-oleoyl-*sn*-glycero-3-phosphocholine. The DOPC 50 system contained the following molecules: 1 phenylalanine dipeptide, 50 DOPC lipids, 2991 TIP3P waters, 8 sodium ions, and 8 chloride ions, for a total of 15,764 atoms. (For this system we used trajectories and data described previously (Lee et al., 2016)). The POPC systems and trajectories were generated in this work. The POPC 50 system contained 1 phenylalanine dipeptide, 50 POPC lipids, 2996 TIP3P waters, 6 sodium ions, and 6 chloride ions, for a total of 15,578 atoms. Finally, the POPC 40 system contained 1 phenylalanine dipeptide, 40 POPC lipids, 2483 TIP3P waters, 7 sodium ions, and 7 chloride ions, for a total of 15,578 atoms. Sodium and chloride ions were added to maintain a physiologically relevant ionic strength. All systems were confined to tetragonal boxes of dimensions: $4.29 \times 4.29 \times 8.30$ nm for DOPC 50, $4.15 \times 4.15 \times 8.74$ nm for POPC 50, $3.70 \times 3.70 \times 8.92$ nm for POPC 40, corresponding to respective lipid headgroup areas of 0.736 nm^2, 0.689 nm^2, and 0.685 nm^2. For the DOPC 50 system, 0.736 nm^2 is in close agreement with an experimental average of 0.723 nm^2 (Liu & Nagle, 2004; Petrache et al., 2004) and the electron density profile is similar to one obtained from X-ray scattering experiments (Lee et al., 2016; Liu & Nagle, 2004). Experimentally, POPC headgroup areas are 0.705 nm^2, which are also close to our simulated values (Leftin et al., 2014). The x and y axes of the simulation box are parallel to the plane of the lipid bilayer, and the z-axis is defined as being perpendicular to the plane of the lipid bilayer. The molecular structures of NAFA, DOPC, and POPC are shown in Figure 1.

MD simulations for the DOPC 50 system were carried out with GROMACS 4.5.4 and simulations for the POPC 50 and POPC 40 systems were carried out with GROMACS 4.5.6 (Pronk et al., 2013). The following options were chosen within GROMACS for all simulations. Forces for DOPC, POPC, and the phenylalanine dipeptide were all represented by the version 36 CHARMM force field (Pastor & MacKerell, 2011; Vanommeslaeghe et al., 2010). Water was represented by using the TIP3P model (Jorgensen et al., 1983). Direct electrostatic interactions were truncated at 1.3 nm and a long-range correction using the Particle Mesh Ewald (PME) method was used (Petersen, 1995). Van der Waals interactions were similarly truncated at 1.2 nm; however, a force switching function was used to smooth the transition between 1.0 and 1.2 nm. A canonical ensemble was used; and, therefore, the number of system particles, the system volume, and temperature were constant. Temperature was held constant at 300 K by using velocity rescaling (Bussi et al., 2007). Initial velocities were sampled from a Maxwell distribution at 300 K. The default leap-frog algorithm was used to integrate the relevant equations of motion with a time step of 2 fs. Periodic boundary conditions in the x, y, and z simulation box directions were used. Constraints on all bonds involving hydrogen atoms were enforced by using the LINCS algorithm (Allen & Tildesley, 1989). Position, energy, and other simulation data were saved every 500-time steps or once every picosecond.

Simulations began by equilibrating each system, as set up by CHARMM-GUI, over 500 ps intervals with the parameters described in the previous paragraph. Once equilibrated, an unrestrained simulation was run for at least 50 ns, and a system image was obtained at $z = 1.6$ nm, corresponding to the dipeptide at the lipid-water interface. This image was then used as the starting point for further umbrella sampling windows in both positive and negative z directions. Umbrella sampling windows for all systems were run from $z = 0.0$ nm to $z = 3.0$ nm in 0.1 nm increments. A harmonic restraining potential of 3000 kJ $mol^{-1} nm^{-1}$, located at the center of each umbrella sampling window, was applied to the center of mass of the phenylalanine dipeptide (Kästner, 2011; Torrie & Valleau, 1977). Each window ran from 50 to 100 ns; as needed, simulation windows near the center of the membrane were extended up to 100 ns to improve statistical overlap for the potential of mean force calculations. The potential of mean force (PMF) was then calculated by using the weighted histogram analysis method (WHAM) (Kumar et al., 1992; Roux, 1995; Souaille & Roux, 2001).

Calculations of position-dependent diffusion constant values D(z) as a function of insertion depth z, were obtained using the method described by Hummer (2005) that is, in turn, based on ideas developed by Zusman (1980) and Bicout and Szabo and based on a numerical solution of the Smoluchowski equation (Bicout & Szabo, 1998). Specifically,

$$D_{n+1/2} = w_{n+1,n}\left[\frac{p^*(n)}{p^*(n+1)}\right]^{1/2} d^2 \tag{1}$$

where n is the bin number, $w_{n+1,n}$ is the transition rate between neighboring histogram bins, p^* is the biased probability distribution, and d is the width of each bin. This approach begins by binning z(t), the distance between the center of mass of the phenylalanine dipeptide and the center of mass of the lipid bilayer, in the entire umbrella sampling simulation window. The biased probability distribution, $p^*(z)$, is then approximated by the resulting, normalized histogram as $p^*(n)$. The average number of transitions between neighboring bins is then calculated from the position time series z(t). Next, $w_{n+1,n}$ is calculated from the average number of transitions between neighboring bins divided by the bin residence time. We chose a bin width of 0.025 nm so that a bin transition is located at the center of any given umbrella window and to minimize error. Under these parameters, the position-dependent translational diffusion coefficient, D(z), for each of our umbrella windows is then found when $n = 1$. Please note: although we are using our harmonically restrained umbrella sampling windows, the diffusion coefficient is calculated at the center of each window where the restraining potential is equal to zero, thereby minimizing the impact of the harmonic umbrella sampling restraint.

Permeation kinetics were then assessed by calculating the permeability coefficient, P, and the mean first passage time (MFPT), $<\tau>$, by using the inhomogeneous solubility diffusion model (Diamond & Katz, 1974). The permeability coefficient is calculated by:

$$P = 1/\int_a^b e^{\beta w(z)} D(z)^{-1} dz \tag{2}$$

where a is a location in the aqueous region on one side of the membrane along the z-axis, b is a location in the aqueous region on the opposite side of the membrane, $\beta = (k_B T)^{-1}$, w(z) is the potential of mean force at a given location along the z-axis, and D(z) is the diffusion constant at a given value of z. The mean first passage time is calculated by (Schulten et al., 1981; Ulander & Haymet, 2003)

$$\langle \tau \rangle = \int_a^b \left[e^{\beta w(z)} D(z)^{-1} \int_a^z e^{-\beta w(z')} dz' \right] dz \tag{3}$$

where all variables are defined in the same manner as for the calculation of P.

A wide variety of additional and smaller data analyses were also conducted. The timescale of molecular motion was investigated at select distances of $z = 0.0$, 0.5, 1.0, 1.5, 2.0 nm by extending the corresponding umbrella windows to 250 ns. Sidechain anisotropy was investigated by defining a vector in the plane of the phenyl group in the phenylalanine dipeptide that is perpendicular to a vector formed by the CG and CZ carbon atoms. A C_2 autocorrelation function for this vector was then calculated. C_2 is a second-order associated Legendre polynomial, defined below, and is related to simple rotational diffusion in 3D space.

$$C_2(t) = \frac{1}{2}\left(3\cos^2\theta(t) - 1\right) \tag{4}$$

where θ(t) is the angle formed between the investigated vector at two different points in time. The rotational correlation time, τ_{rot}, was then determined by fitting the C_2 autocorrelation function to a single exponential decay function, to obtain an average time, or to a double exponential, to obtain weights and timescales of slower and faster

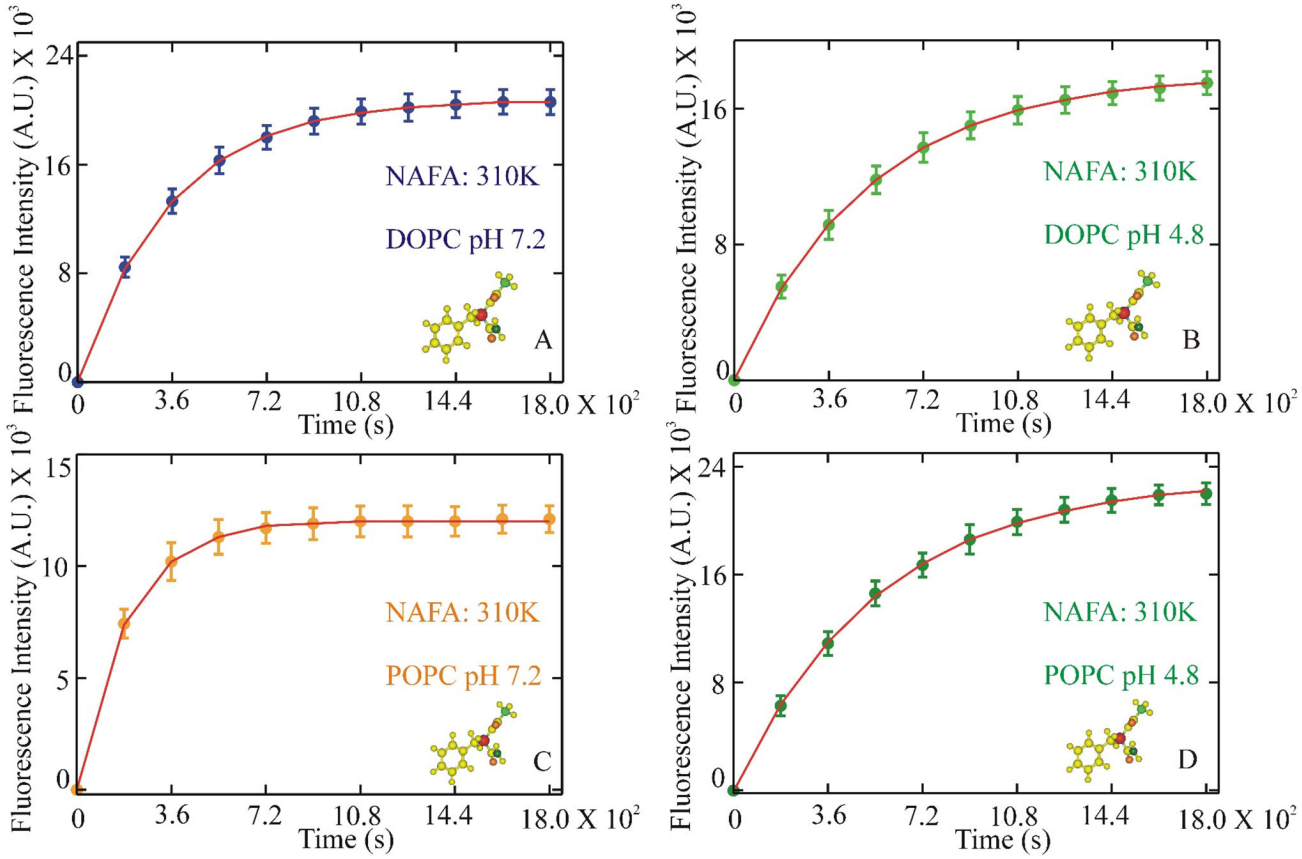

4.8, NAFA translocation rate in DOPC and POPC does not vary significantly.

Figure 2. Integrated fluorescence intensity of NAFA with respect to time at 310 K (A) in DOPC at pH 7.2. (B) in DOPC at pH 4.8. (C) in POPC at pH 7.2 (D) in POPC at pH 4.8. The results shown are averages and standard deviations from three replicates.

components. Similarly, the autocorrelation time for the projection of the insertion vector along the z-axis was determined. Backbone and sidechain conformational angles, radial distribution functions, solvent accessible surface areas, and the radius of gyration were calculated by using the relevant GROMACS 4.5.6 tools (Pronk et al., 2013). The dihedral angle clustering analysis was done with CHARMM (Brooks et al., 2009). The membrane electron density profile was calculated with the density tool of GROMACS, which starts with trajectory average atomic densities and assigns the number of electrons based on atomic number (Pronk et al., 2013).

Results and discussion

Experimental results

Unassisted permeation of NAFA was determined across DOPC and POPC lipids over a period of 30 hrs. The rate of NAFA transport was determined by fitting the kinetic profile generated with the fluorescence intensity change as a function of time. These experiments were performed at 310 K and two different pH environments, pH 4.8, and pH 7.2. Lucifer yellow and Cresyl blue were used as positive and negative controls, respectively. The integrated fluorescence intensities as a function of time were plotted to obtain the rate of transport in each case (presented in Figure 2(A–D)). The observed rates are in hours are found to vary significantly at neutral pH in both DOPC and POPC. The rate of translocation for NAFA in DOPC is observed to be significantly slower, almost by a factor of two, in comparison with POPC at pH 7.2. In an acidic environment, pH 4.8, NAFA translocation rate in DOPC and POPC does not vary significantly.

There is a measurable dependency of the time scale on lipid type and pH. It is important to note that at neutral pH 7.2 and in POPC NAFA transport is faster by a factor of two compared to DOPC, 3 h, and 6 h, respectively. In an acidic pH 4.8, there is a very negligible difference in the rate of NAFA in both POPC and DOPC, ~8 h. This suggests that the protonated environment hinders the transport rate of NAFA in POPC, whereas in DOPC rates vary negligibly in two different ionic conditions.

Potential of mean force

The potential of mean force represents the free energy required to reversibly pull the dipeptide along the z-axis relative to the membrane center of mass. The potential of mean force in the aqueous region at 3.0 nm, corresponding to the dipeptide in the solution phase, for each system was defined as 0.0 kJ mol^{-1} and all other values are calculated relative to this reference. The phenylalanine dipeptide exhibits very similar behavior in all three systems, as seen in Figure 3: a free energy minimum around the lipid-water interface and a free energy barrier at the center of the membrane. The

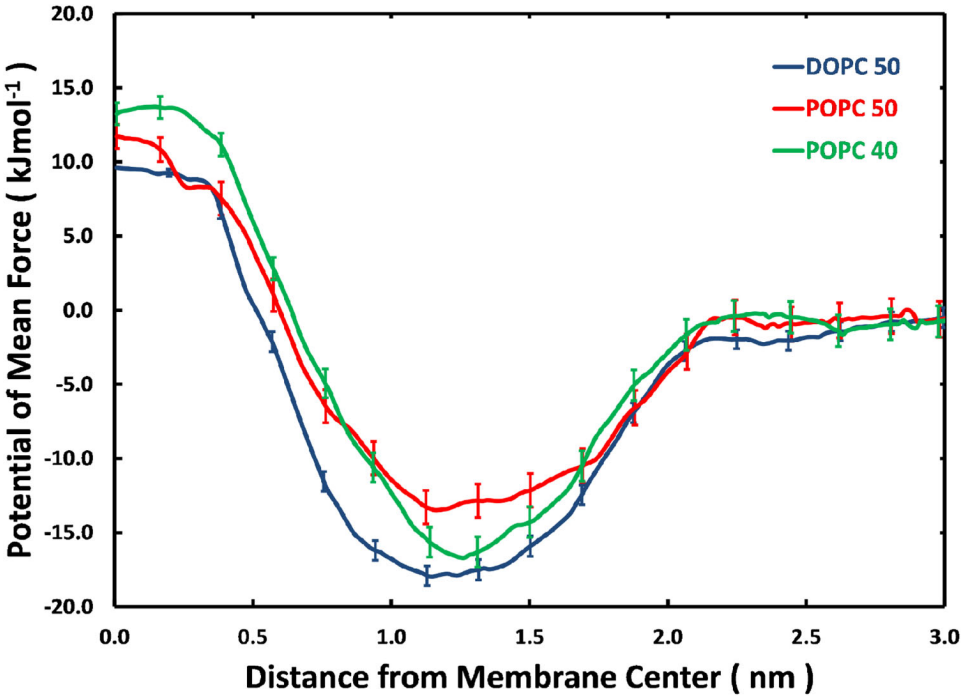

Figure 3. The free energy required to pull the phenylalanine dipeptide along the z-axis of the simulation box is plotted below as the potential of mean force. $Z = 0$ represents the center of the lipid bilayer. A 95% confidence interval representing the standard error is also plotted for select points as determined by the Bootstrap method.

minima are −16, −13, and −18 kJmol^{-1}, respectively, for the POPC 40, POPC 50, and DOPC 50 systems, and occur at 1.3, 1.2, and 1.2 nm. The free energy barriers are 14, 12, and 10 kJ mol^{-1}, in the same order as before. Qualitatively, these results are very similar to findings for other amino acids and agree with our previous studies concerning aromatic dipeptides (Cardenas et al., 2012; Lee et al., 2016) Blocked phenylalanine contains a hydrophilic backbone and a hydrophobic side chain which results in a smaller free energy near the membrane interface where the backbone can interact with the aqueous region at larger z-values and where the side-chain can interact with the lipid environment at smaller z-values.

The PMFs for POPC 40 and POPC 50 demonstrated little difference at the center of the membrane; however, POPC 40 demonstrates a small, but statistically significant difference at the interface. Although the effect of lipid bilayer size on aromatic dipeptide PMFs has not been examined before, Nitschke *et. al.* has conducted membrane size studies on methanol and ibuprofen with POPC bilayers (Jo et al., 2007). Even though ibuprofen is less polar and is, therefore, more likely to pass through a lipid bilayer (Jo et al., 2007), it still contains a similar combination of polar and nonpolar moieties and produces the same qualitative PMF shape as the phenylalanine dipeptide. In Nitschke's analysis (Nitschke et al., 2016), lipid size may influence the PMF by three key mechanisms: 1.) averaging out the effects of membrane fluctuations, 2.) finite-size effects altering the lipid structure, and 3.) solute stabilization through the interaction of periodic images. They determined that only membrane fluctuations influence the PMF for lipid bilayers as small as 32 molecules. For example, the central barrier for ibuprofen is lowered by 3 kJ mol^{-1} when the system size is increased from 32 to 50 lipids. In our case, the PMF is lowered 2 kJ mol^{-1} when the system size is increased from 40 to 50 lipid molecules, in good agreement with Nitschke's results. In the interfacial region, the PMF is lowered by 5 kJ mol^{-1} for ibuprofen and by 3 kJ mol^{-1} for the phenylalanine dipeptide. Interestingly, these system size-effects can be removed by utilizing a cylinder-based center of mass coordinate, rather than the all lipid center of mass coordinate that we use (Carpenter et al., 2014). Alternatively, the small variation of the PMF due to system size may be due to the relatively short simulation length: 20 ns per window for Nitschke and 50 ns per window for our results. The passive transport of a peptide through a lipid bilayer heavily depends on membrane fluctuations at the interface, which may not be adequately sampled in short simulations of small numbers of lipids, producing a systematic bias towards smaller, less negative, interfacial energies (Klauda et al., 2008). For example, lipid molecules can flip from one side to another on the scale of hundreds of nanoseconds (Wei & Pohorille, 2014), lipid defects and void spaces form in the center of the membrane on the order of tens of microseconds (Neale et al., 2011), and, rotational energy barriers can further complicate matters by occurring on the order of tens of nanoseconds (Cardenas & Elber, 2013; Klauda et al., 2008).

The DOPC 50 PMF exhibits a significantly smaller central barrier and a broader interfacial minimum than the POPC 50 curve, with particularly large deviations within the region between 0.6 and 1.0 nm, as shown in Figure 3. Traditionally, the width of the PMF near the interfacial minimum has been associated with the ability of the lipid membrane to either exclude polar solutes or to enfold apolar solutes due to membrane fluctuations (Comer, Schulten, et al., 2014). Since our simulations use the same solute for each lipid bilayer

Table 1. Summary of computational estimates of membrane permeability from NAFA simulations. Permeation coefficients P are in cm s^{-1} and mean first passage times (MFPT) in s.

System	P	MFPT
POPC 50	0.82 ± 0.03 cm s^{-1}	$(9.1 \pm 0.5) \times 10^{-6}$ s
POPC 40	0.24 ± 0.003 cm s^{-1}	$(1.2 \pm 0.9) \times 10^{-6}$ s
DOPC 50	0.66 ± 0.03 cm s^{-1}	$(4.1 \pm 0.3) \times 10^{-6}$s

system, the calculated PMF differences must be due to differences in bilayer properties. DOPC contains an additional double bond in its aliphatic tail as compared to POPC. This greater lack of saturation causes the DOPC bilayer to be less ordered than POPC and other saturated phospholipids (Mills et al., 2008). Our results suggest that the less ordered DOPC bilayer is more easily capable of undergoing distortions that better accommodate the amphiphilic nature of the phenylalanine dipeptide, thereby producing a broader PMF curve near the interfacial free energy minimum. These membrane distortions either allow the hydrophilic moiety to remain in contact with the bulk aqueous region (Vaz & Almeida, 1991) or allow the partial retention of the solvation shell at a greater insertion depth, thereby lowering the free energy. These effects are discussed in greater detail in some of the following sections.

Translational diffusion

The translational diffusion in all three systems closely follows our previously described results for aromatic amino acids in DOPC 50 (Lee et al., 2016). In the aqueous region, the phenylalanine dipeptide exhibits diffusion constants of $5.20 \pm 0.10 \times 10^{-10}$ m^2s^{-1} in DOPC 50, $5.40 \pm 0.15 \times 10^{-10}$ m^2s^{-1} in POPC 50, and $5.23 \pm 0.15 \times 10^{-10}$ m^2s^{-1} in POPC 40. All these values possess overlapping confidence intervals, and any differences are statistically insignificant. At the membrane interface at $z = 1.5$ nm, diffusion constants of $4.82 \pm 0.17 \times 10^{-10}$ m^2s^{-1} in DOPC 50, $4.86 \pm 0.089 \times 10^{-10}$ m^2s^{-1} in POPC 50, and $4.83 \pm 0.15 \times 10^{-10}$ m^2s^{-1} in POPC 40 were determined. Again, these values are not statistically different from each other. However, they are slightly smaller than the values determined within the aqueous region. Finally, at the center of the membrane, the phenylalanine dipeptide diffusion constants are $5.63 \pm 0.26 \times 10^{-10}$ m^2s^{-1} for DOPC 50, $5.46 \pm 0.17 \times 10^{-10}$ m^2s^{-1} for POPC 50, and $5.48 \pm 0.15 \times 10^{-10}$ m^2s^{-1} for POPC 40. Here, as well, the results for the three systems are not statistically different from each other, and they are similar to the values within the aqueous region. This pattern of slightly smaller diffusion constants near the membrane interface as compared to either the membrane interior or aqueous regions has also been found in many different molecules from water to organic solvents to small pharmaceutical compounds (Khuntawee et al., 2015). The observed differences are most pronounced for polar and amphiphilic molecules and negligible for larger, more nonpolar molecules (Xiang & Anderson, 2006). While most of the D(z) values follow relatively smooth variation with insertion depth z, there are two data points with significant deviations, for POPC 40 at 1.6 nm and DOPC 50 at 1.7 nm. In summary, switching from DOPC to POPC or from 50 to 40 lipid molecules does not have a measurable impact on the position-dependent translational diffusion constants.

Permeability measures

The permeation coefficient – an important quantity used in pharmacokinetic analyses – and the mean first passage time (MFPT) are discussed in this section, with a summary presented in Table 1. Both quantities represent a more physically relevant interpretation of our diffusion constant and potential of mean force data. The MFPT for the phenylalanine dipeptide through a POPC 50, POPC 40, and DOPC 50 membrane system are $(9.1 \pm 0.5) \times 10^{-6}$ s, $(1.2 \pm 0.9) \times 10^{-6}$ s, and $(4.1 \pm 0.3) \times 10^{-6}$ s, respectively, by using Equation (3). The given 95% confidence intervals were calculated by propagating error from the diffusion and potential of mean force data displayed in Figures 3 and 4. All of the passage times were on the order of microseconds, which is in agreement with similar computational studies on molecules around the same size as the phenylalanine dipeptide (Diamond & Katz, 1974). Of the three systems studied, POPC 40 has the largest passage time, POPC 50 the smallest, and DOPC 50 in between the two. These calculations are most sensitive to the permeant environment near the center of the membrane and therefore reflect the potential of mean force and diffusion constant around $z = 0$ nm. The diffusion constants near the center of the membrane are largely the same for all three systems; however, the PMF is greatest for POPC 40, followed by POPC 50, and then DOPC 50, which matches the qualitative order of the MFPT. It is interesting to note that the width and depth of the PMF did not have a substantial impact on this ordering since the PMF for DOPC 50 is much deeper and broader than for POPC 50.

Our calculated permeation coefficients for the POPC 50, POPC 40, and DOPC 50 systems are, respectively: 0.82 ± 0.03 cm s^{-1}, 0.24 ± 0.03 cm s^{-1}, and 0.66 ± 0.03 cm s^{-1} by using Equation (2). Again, the reported uncertainties are 95% confidence intervals determined through the propagation of error in the PMF and diffusion constant data. It should also be noted that these calculations are highly sensitive to the choice of the free energy in the aqueous region; for example, differences of only a few kJmol^{-1} resulted in order of magnitude differences in the permeation constant. Therefore, actual uncertainties are likely far larger, and care should be taken in terms of converging the aqueous PMF. The MFPT calculations are not sensitive to this variation and maybe a more accurate reflection of the permeation kinetics. As a result, the relatively small differences in the permeation coefficients for each system are not significant. In general, these permeation coefficients agree with other simulations with small molecules (Orsi et al., 2009). We previously reported experimental coefficients for the phenylalanine dipeptide in DOPC 50 of 5.6×10^{-8} cm s^{-1}(Lee et al., 2016), as compared to our computational value in this work of 0.66 cm s^{-1}. As expected, the computational value is far larger than the experimental result due to any of the following factors which have been well documented in the literature: the

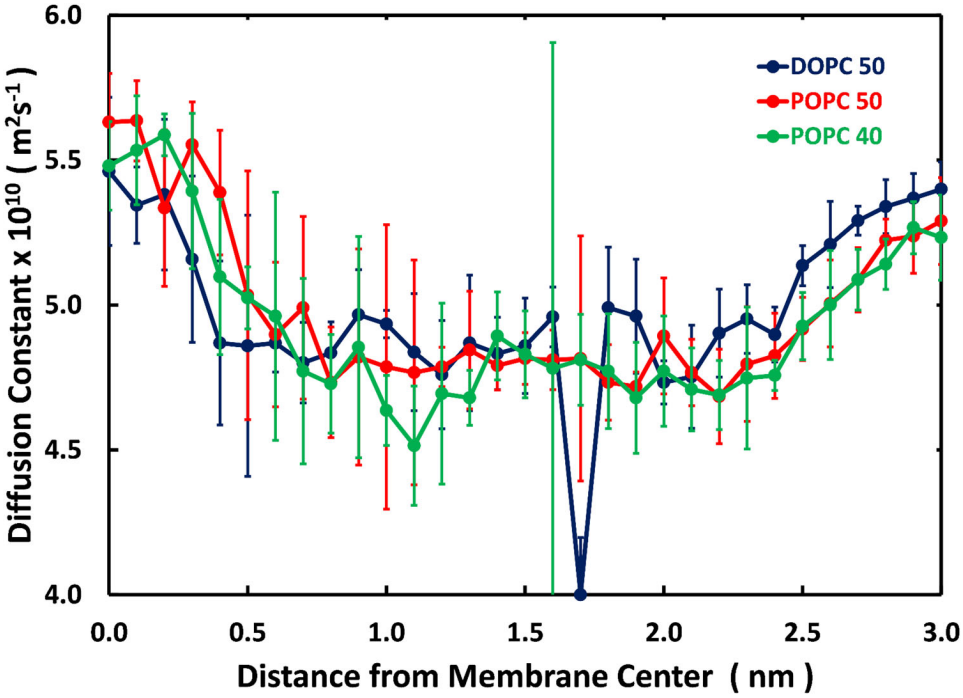

Figure 4. Translational diffusion constants of the NAFA dipeptide as a function of distance from the center of mass of the lipid bilayer are depicted. These constants were determined by a numerical solution of the Smoluchowski equation. The error bars represent the standard error at a 95% confidence level, as calculated by separating the data for each simulation window up into four consecutive bins.

use of the inhomogenous solubility-diffusion model (Comer, Phillips, et al., 2014; Parisio et al., 2013), hidden rotational barriers (Jämbeck & Lyubartsev, 2013), membrane, and solvent fluctuations (Cardenas & Elber, 2014), and the choice of force field (Cardenas et al., 2012; Lee et al., 2016).

Rotational sidechain diffusion

In contrast to the largely flat translational diffusion profile in Figure 4, the NAFA rotational diffusion is significantly slowed within the lipid bilayers. As previously reported, in the DOPC 50 system the average rotational correlation time of the sidechain phenyl group was ca. 0.3 ns in the membrane center ($z = 0$), 2 ns in lipid headgroup region ($z = 1$ nm) and 1 ns at the solvent/lipid interface ($z = 2$ nm) (Lee et al., 2016). In POPC 40 the corresponding results were 0.2, 1.4 and 0.4 ns, respectively, while in POPC 50 values were 0.1, 1.2 and 0.4 ns, respectively. Overall, there is a trend for slower reorientations inside the membrane in the smaller POPC 40 system relative to the larger POPC 50, and faster reorientations in POPC relative to DOPC. However, qualitative comparisons of data between different simulation systems and umbrella sampling windows are difficult. The $C_2(t)$ decays are mostly not well described by single exponentials. In many cases, very long tails are present, with estimated time scales in the tens to hundreds of ns, which cannot be reliably fitted given our simulation time scales. Finally, in several cases the correlation functions do not decay to zero, indicating small effects of even longer-term processes. The general effect is qualitatively similar in all three simulations: a dramatic slowing down of rotational diffusion in the head group region, and a somewhat smaller slowdown in the center and membrane interface. Measured NAFA reorientation times are substantially longer than previously reported values for the phenylalanine dipeptide in water with MD. In MD it was found to be 20 ps applying CHARMM force field and TIP3P water at 300 K (Kuczera et al., 2010) and the corresponding measured value was 98 ± 30 ps at 278 K. This may suggest that the reorientation motion of the sidechain plays an important role in the transport process.

Insertion angle

The insertion vector of each peptide is defined by an angle, θ, between two vectors: one vector points along the positive z-axis with respect to the lipid membrane, and the other vector starts from the center of mass of the backbone and ends at the center of mass of the sidechain. In other words, an angle of 0° indicates that the sidechain is pointing in the positive z-direction and the backbone in the negative z-direction. Alternatively, an angle of 180° represents the reverse: the peptide backbone is pointing in the positive z-direction, and the sidechain is pointing in the negative z-direction.

From Figure 5, peptide orientations are largely homogenous in the aqueous region beyond 2.0 nm. However, as the peptide nears the membrane interface, the insertion angle prefers large values between 120° and 180°, indicating a preference for the sidechain to enter the membrane first. The sidechain, particularly for phenylalanine, is largely non-polar and prefers to interact with the non-polar aliphatic groups within the lipid membrane, while the polar amide and acetate groups within the peptide backbone prefer interactions with the solvent. This preference continues until around 0.3 to 0.4 nm from the center of the membrane, where the insertion angle can, once again, adopt a wide range of different values. At the center of the membrane,

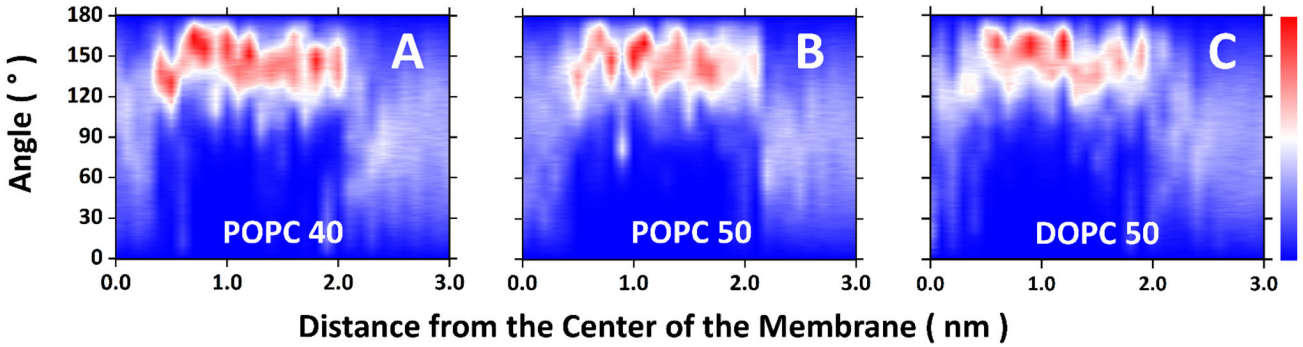

Figure 5. The insertion angle of the NAFA dipeptide as a function of the distance from the center of the lipid membrane can be seen below. The insertion vector points from the backbone center of mass to the sidechain center of mass. The insertion angle, θ, is then the angle in between the insertion vector and the positive z-axis. Blue regions represent areas of low, normalized probability, and red regions represent areas of high, normalized probability as a function of θ and the distance from membrane center, z.

the local environment is similar in both the positive or negative z-direction, and a preference for one angle or direction is unlikely to be seen in this homogenous region. The ability of NAFA to change its orientation in either the positive or negative z-direction is very similar to the results found in previous studies of aromatic dipeptides (Cardenas & Elber, 2013). Both lipid types, POPC and DOPC, and system sizes, POPC 40 and POPC 50 exhibit very similar results.

The timescale of the reorientation of the insertion vector was also examined by calculating the autocorrelation function for the projection of this vector along the z-axis, also known as the cosine of the insertion angle. Most interesting is the value at $z = 0$, in the membrane center, for which 1.8 ns was obtained for POPC 40 and 1.0 ns for POPC 50. This indicates that the whole peptide has readily changed orientation at the mid-point of the membrane permeation path. Estimation of insertion angle reorientations at other locations in the membrane give times that are much slower than 1 ns and are highly speculative, as complete sampling was not obtained on our simulation time scale, similarly to some of the sidechain reorientations discussed above. These longer timescales are likely due to the large-scale fluctuations of the lipid molecules within the membrane, which are absent at the center of the membrane (Neale et al., 2011). Conversely, the smaller autocorrelation times at the center are due to the creation of transient void spaces because of the greater disorder of the lipid tails (Vaz & Almeida, 1991). These void spaces then allow NAFA to rotate with greater freedom. It bears mentioning again: translational diffusion is largely independent of the permeation depth; sidechain rotation begins to show a somewhat scattered dependence on z; and, finally, the rotation of the entire molecule, as shown here, clearly depends on the location of the permeant within the membrane.

Backbone conformations

Figure 6 contains Ramachandran plots for each of the systems studied (Ramachandran et al., 1963). Simulations were split up into three regions: the water region at the far edge of the simulation box, the interface where the lipid headgroups interact with the aqueous region, and the center of the membrane where the lipid tails interact, as seen in Figure 6(A). Figures 6(B–D) contain plots of all three slices for the POPC 40, POPC 50, and DOPC 50 systems. The sample structures around the Ramachandran plot are depictions of the two most prevalent conformations, representing around 80% or greater of all observed clusters. In the aqueous region, all three systems sample three conformational areas: the α-helical region with negative Φ and Ψ angles, the β-sheet area with negative Φ and positive Ψ angles in the top corner, and the small region sandwiched in-between the α-helices and β-sheets, representing a C_{7eq} conformation, a free energy minimum that is commonly found in dipeptides and includes an internal backbone hydrogen bond between the terminal blocking groups (Tobias & Brooks, 1992). These findings are similar to what we found for the other aromatic dipeptides of tyrosine and tryptophan in the aqueous region (Lee et al., 2016). At the interface, the α-helix and β-sheet regions lose probability density to the C_{7eq} conformation until, eventually, at the center of the membrane, only the C_{7eq} conformation remains to a significant degree. This demonstrates that the phenylalanine dipeptide adopts different conformations as it travels through the membrane. This behavior is consistent regardless of system size or lipid type, as explored in greater detail throughout the clustering analysis in the next section.

Sidechain conformations

The two sidechain dihedral angles, χ_1 and χ_2 were plotted in Figure 7 in the same manner as the Ramachandran plots in Figure 6. By looking at the top χ_1- χ_2 plot in Figure 7(A) for the aqueous region, the phenyl ring of the phenylalanine dipeptide in DOPC 50 samples six different conformers: tg^+, g^-g^+, and g^+g^+ in the top row; and tg^-, g^-g^-, and g^+g^- in the bottom row. However, only tg^+, g^-g^+, tg^-, and g^-g^- are heavily sampled, as indicated by the large, red regions. g^+g^+ and g^+g^- are only weakly sampled due to the much smaller, less intense, and whiter regions on the right-hand side of the panel. Note: this nomenclature follows the standard convention for the naming of amino acid sidechain conformations. For example, tg^+ refers to a *trans* χ_1 dihedral angle around 180° and a *gauche(+)* χ_2 dihedral angle around +60°. In the interfacial region of Figure 7(A), the four heavily sampled

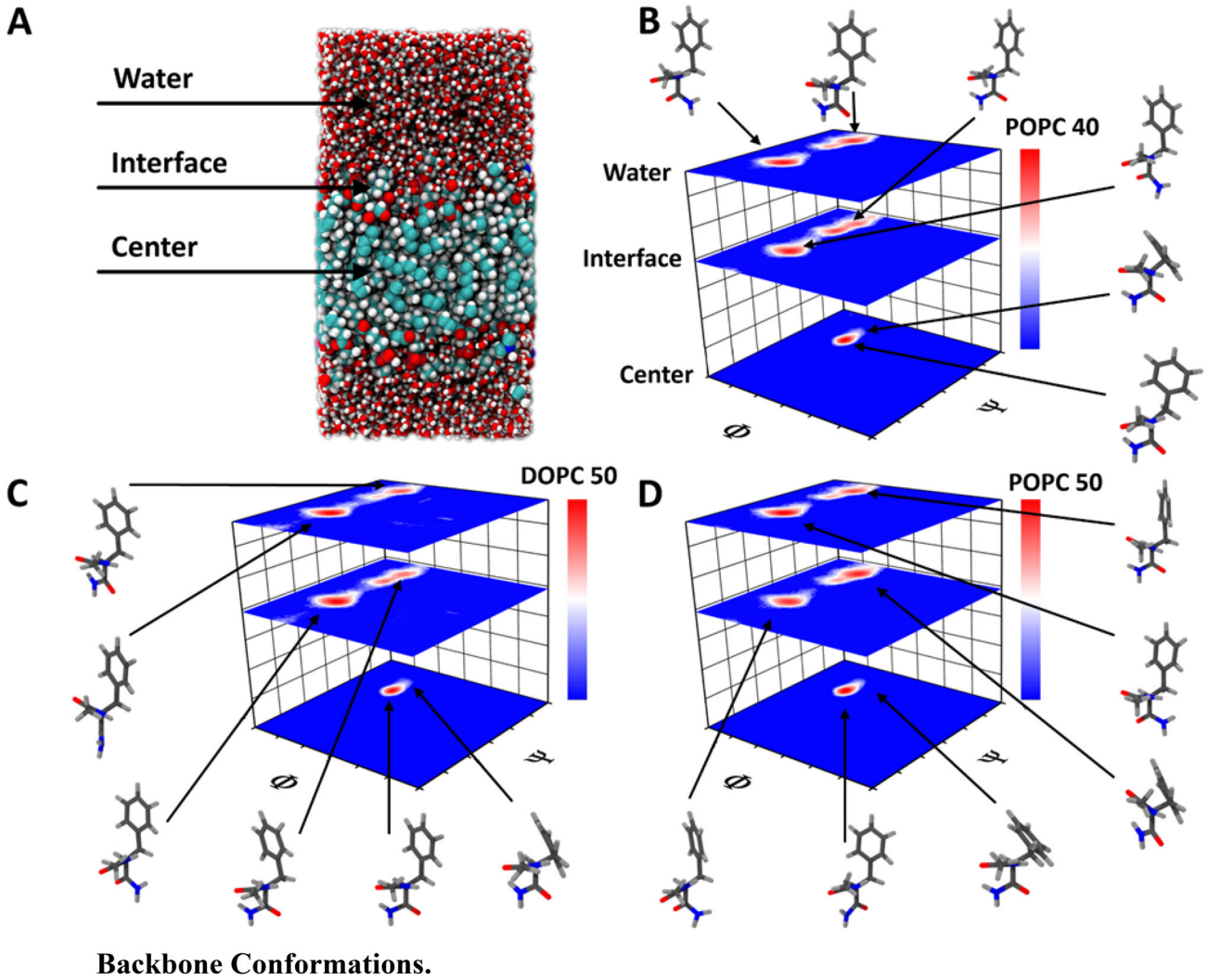

Figure 6. Shows Ramachandran plots, with probability distribution of backbone Φ and Ψ dihedral angles, for each of the studied system. Simulations were split up into three regions: the water region at the far edge of the simulation box, the interface where the lipid headgroups interact with the aqueous region, and the center of the membrane where the lipid tails interact, as seen in 6A. 6B–D contains Ramachandran plots of all three slices for the POPC 40, POPC 50, and DOPC 50 systems.

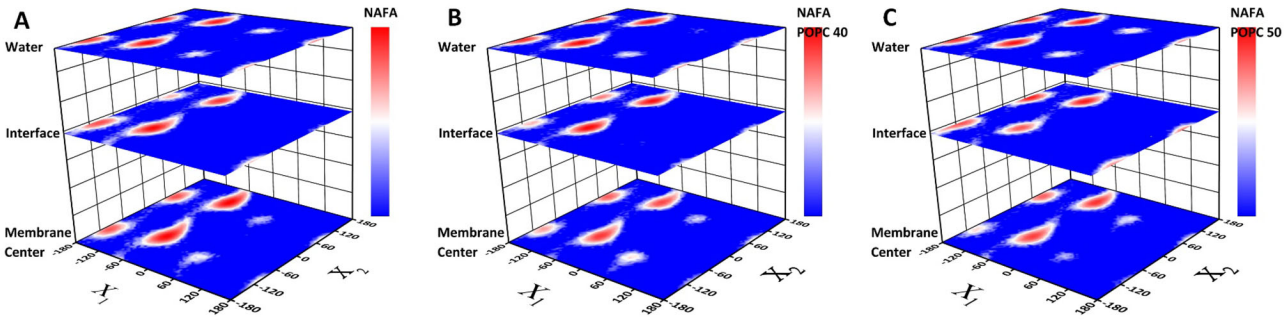

Figure 7. χ_1 and χ_2 sidechain angles for the phenylalanine dipeptide in 7A represents three such plots at the center, interfacial, and aqueous regions, in ascending order, for the simulations of the phenylalanine dipeptide with 50 DOPC lipids. Blue represents regions where the binned probability distribution is very small or zero; whereas, red indicates a large likelihood that the sidechain will adopt that particular conformation. 7B is the same as 7A, except a membrane consisting of 40 POPC lipids was used; and, finally, 7C represents the same type of plot where 50 POPC lipids were used within the membrane.

conformations are still present; however, g^+g^+ and g^+g^- vanish completely before reappearing within the center of the membrane. This phenomenon was also present in POPC 40 and POPC 50, as seen in Figure 7(B, C). Although the dihedral sidechain angles do not play as important a role in membrane permeation as the backbone, there is a slight conformational preference in the interfacial region against g^+g^+ and g^+g^-. In terms of membrane size, the g^+g^+ conformer is largely absent in the aqueous region of the POPC 40 system and slightly more prevalent in POPC 50. Finally, there is little difference between the DOPC 50 and POPC 40 systems.

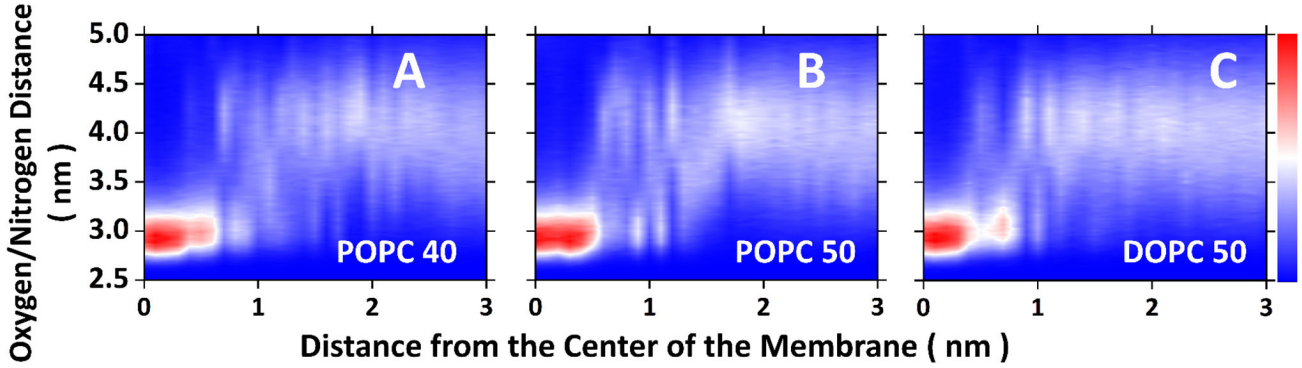

Figure 8. The distance between the oxygen and nitrogen atoms of the respective blocking groups – the oxygen atom of the acetylated N-terminus and the nitrogen atom of the amidated C-terminus – are plotted for each simulation window in terms of their associated probability distributions. Blue represents a small or zero likelihood of the phenylalanine dipeptide adopting a conformation with that particular oxygen/nitrogen distance, whereas red indicates a high likelihood.

In Figure 7, χ_1 and χ_2 sidechain angles for the phenylalanine dipeptide are displayed in the same manner as the previously examined Ramachandran plots. Specifically, Figure 7(A) represents three such plots at the center, interfacial, and aqueous regions, in ascending order, for the simulations of the phenylalanine dipeptide with 50 DOPC lipids. Blue represents regions where the binned probability distribution is very small or zero; whereas red indicates a large likelihood that the sidechain conformations will adopt that particular conformation. Figure 7(B) is the same as 7A, except a membrane consisting of 40 POPC lipids was used; and, finally, 7C represents the same type of plot where 50 POPC lipids were used within the membrane.

Peptide structures and clustering

A clustering analysis of the Φ, Ψ, χ_1, and χ_2 dihedral angles was conducted for structures at the center of the membrane, interface, and water regions. As we previously reported (Lee et al., 2016), the phenylalanine dipeptide in a 50 DOPC membrane system adopts seven clusters in the water region: 4 α and 3 β; four at the interface: 2 α and 2C_{7eq}-β hybrids; and four at the center of the membrane: 2C_{7eq} and 2 β. Please note that clusters were classified based on those identified by Tobias and Brooks (1992) to within a tolerance of around 10° in the Φ dihedral angle and around 20° in the Ψ angle.100 Also, the two most prevalent structures within each clustering region are depicted in the margins of panels B, C, and D in Figure 6. In the 50 POPC lipid membrane system, seven clusters were identified in the water region: 3 α and 4 β; four at the interface: 2 α and 2 β; and five at the center: 2C_{7eq}, 2 β, and 1C_{7eq}-β hybrid. In the 40 POPC lipid membrane system, ten clusters were identified in the water region: 5 α and 5 β; four at the interface: 2 α and 2 β; and five at the center: 2C_{7eq}, 2 β, and 1 distorted C_{7eq} cluster. The larger number of clusters in the water region for this system was surprising; however, all the additional clusters beyond the original seven identified for the DOPC 50 and POPC 50 systems represented fewer than 0.5% of the total cluster representation. More interestingly, the interfacial region of the

POPC systems had only α and β clusters; however, the DOPC interfacial region contains two β clusters whose Ψ angles are halfway between a typical β or C_{7eq} cluster, hence their designation as C_{7eq}-β hybrids. These hybrid clusters may indicate that the phenylalanine dipeptide is being forced into lower-energy conformations sooner.

Indeed, the oxygen-to-nitrogen atom distances on the terminal blocking groups, as plotted in Figure 8, indicate that these two atoms are coming closer together to form a lower energy C_{7eq} cluster at a z-distance of 0.7 nm, whereas the POPC systems do not begin this process until around 0.5 or 0.6 nm. In the water region, all systems adopt an oxygen/nitrogen distance between 3 to 5 nm and do not exhibit a strong preference. However, at the center of the membrane, all lipids and sizes indicate a strong preference for a very small oxygen/nitrogen distance around 2.8 to 3.1 nm as the polar dipeptide backbone attempts to either minimize its interfacial free-energy with respect to the non-polar environment at the membrane center or to potentially maximize their dipole or hydrogen bonding interactions.

Molecule shapes and sizes

All three systems indicate little variation in both the radius of gyration (R_g) and the solvent-accessible surface area (SASA) of the phenylalanine dipeptide with depth of lipid insertion (data not shown). This is not surprising due to the small size of the peptide.

Specific interactions

The phenylalanine dipeptide interacts with a different environment at varying distances from the center of the model DOPC or POPC membrane. The number of water molecules within 0.3 nm of any part of the dipeptide is plotted in Figure 9. In the aqueous region 3.0 nm from the center of the model membranes, all three peptides were surrounded by around 45 water molecules, with the POPC and DOPC 50 systems at nearly the same value; whereas, the POPC 40 system has a slightly larger number. As the dipeptide moves closer to the membrane interface, the number of closely coordinated water molecules gradually decreases to around 20 at $z = 1.5$ nm.

As expected for relatively small and non-ionic permeants, there are few, if any, water molecules surrounding the

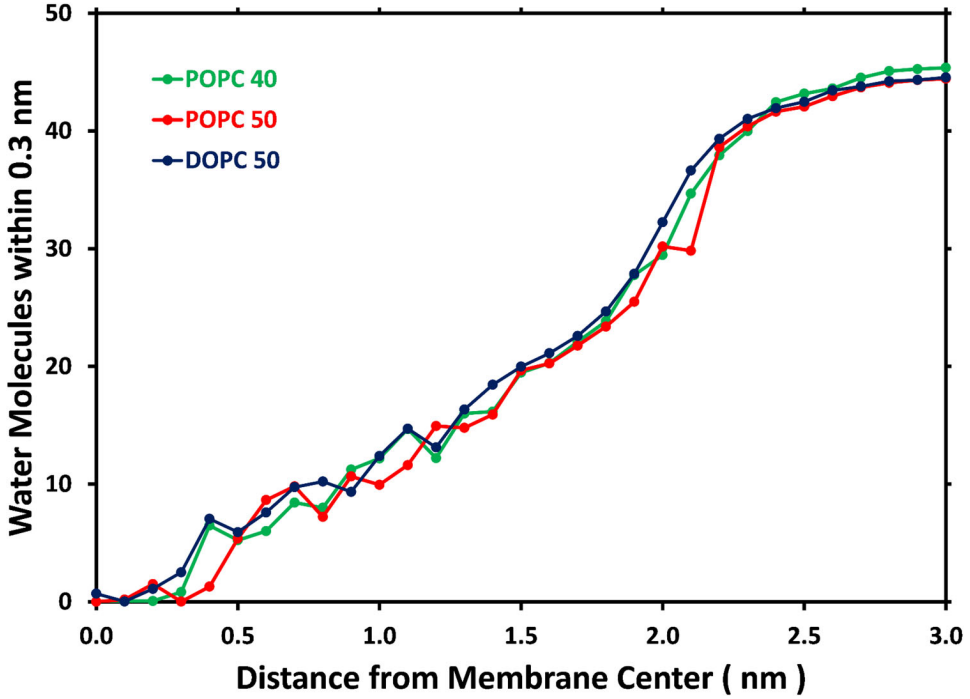

Figure 9. The number of water molecules within 0.3 nm of the phenylalanine dipeptide in all three membrane systems is displayed. At each membrane position, the standard error of the sample mean was calculated at a 95% confidence level and was less than 0.06 water molecules – too small to appear on this figure.

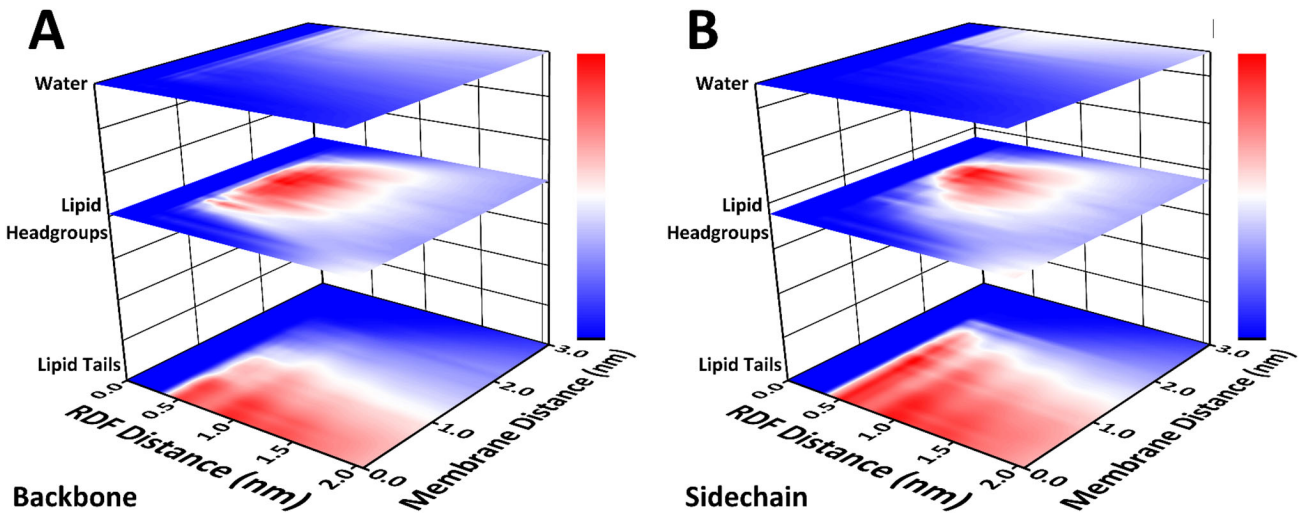

Figure 10. Radial distribution functions for either the peptide backbone or the peptide sidechain with water, lipid headgroups, and lipid tails are plotted at different NAFA insertion depths. Data shown is for POPC 50 systems; results for DOPC 50 and POPC 40 are highly similar and are not shown.

dipeptide at the center of the membrane. However, it is interesting to note that at $z = 0.0$ nm from the membrane center, the DOPC 50, POPC 50, and POPC 40 systems possess the following number of nearby water molecules: 0.690 ± 0.007, 0.006 ± 0.124, 0.006 ± 0.114. The numbers for the POPC systems are essentially zero; however, the DOPC 50 system is statistically above zero. This may indicate a slightly greater permeability for the DOPC system due to its less ordered lipid tails.

Radial distribution functions (RDF) between either the backbone or sidechain moiety of the phenylalanine dipeptide interacting with the non-hydrogen atom components of water, the lipid tails, or the remaining lipid headgroup atoms for the POPC 50 system are plotted in Figure 10. The corresponding figures for the DOPC 50 and POPC 40 systems are not included since they are indistinguishable to any but the most discerning eye. At the top of panel 10 A and panel 10B, both moieties of the peptide are surrounded by a relatively uniform distribution of water molecules. However, this uniformity comes to a gradual stop at 2.0 nm from the membrane center for the sidechain, whereas, the backbone continues to interact with the aqueous region until a distance of 1.0 nm. This trend is corroborated by the insertion angle data in Figure 5 where the peptide backbone remains oriented towards the aqueous region at greater membrane insertion depths. Similarly, both peptide moieties strongly associate with the lipid headgroups in the interfacial regions between 0.8 and 2.0 nm; however, the sidechain possesses a more

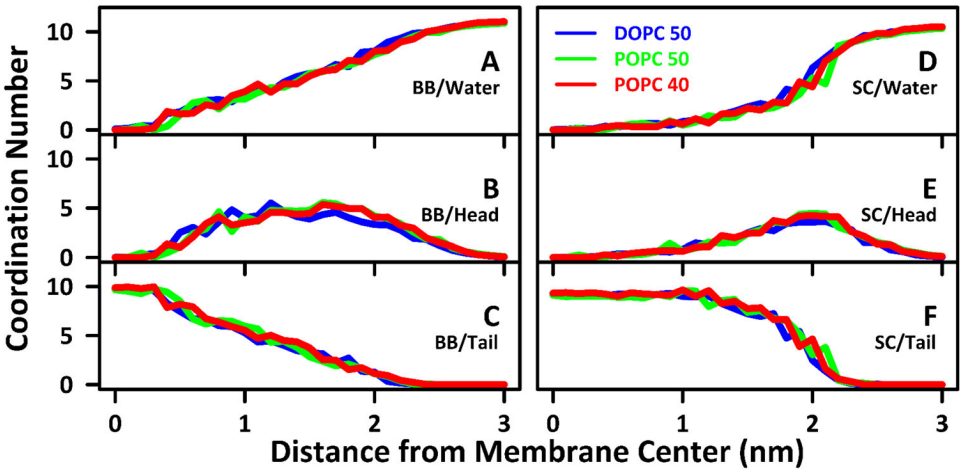

Figure 11. Coordination numbers are displayed and represent the average number of the specified sub-groups within 0.5 nm of either the dipeptide backbone or sidechain. The peptide sidechain was defined as all the non-hydrogen atoms of the phenylalanine R-group, and the backbone consists of the remaining non-hydrogen atoms in the dipeptide, including those of the terminal blocking groups. Sub-groups were defined, as follows: water, lipid oxygen atoms; lipid tail, all of the carbon atoms in the acyl group of the lipid; lipid headgroup, all of the non-hydrogen and non-tail atoms remaining in the lipid. Panel 11A displays the coordinating number of water groups around the backbone; Panel 11B, the backbone, and lipid headgroups; Panel 11C, the backbone and lipid tails; Panel 11D, the sidechain, and water; Panel 11E, the sidechain and lipid headgroups; Panel 11F, the sidechain and lipid tails.

abrupt transition away from the lipid headgroups at 1.0 nm, as opposed to 0.4 nm for the backbone. Finally, the opposite trend is noticed with the lipid tails: the sidechain remains closer to them over a greater membrane distance (0.0 to 1.9 nm); whereas, the backbone strongly associates with the tail groups near the membrane center (0.0 to 1.0 nm.)

Coordination numbers representing the average number of atoms belonging to each of the previously mentioned groups within 0.5 nm of the backbone or sidechain are plotted in Figure 11. In Figure 11(A), the coordination number between water and the backbone gradually decreases; however, in Figure 11(D), the sidechain undergoes a more distinct transition and rapidly loses coordinating water atoms at 2.1 nm. In Figure 11(B), the backbone is coordinated by a significant number of headgroup-atoms over a large distance (0.6 to 2.5 nm) as compared to the sidechain (1.7 to 2.2 nm) in panel 11E. Finally, the sidechain rapidly associates with the lipid tails at around 2.0 nm, in Figure 11(F), before completing said transition at 1.0 nm; whereas, the backbone undergoes a more gradual process. Again, this matches both the RDF and z-insertion angle data demonstrating that the phenylalanine sidechain enters the membrane first, and the backbone follows. Interestingly, there is not a significant difference in coordination number between the choice of lipid type (DOPC 50 in blue as compared to POPC 50 in green) or system size (POPC 50 in green and POPC 40 in red).

Conclusions

In this investigation, we have carried out both experiments and computer simulations to better understand the passive membrane transport of a neutral aromatic dipeptide, NAFA in two types of lipid bilayers, DOPC and POPC. Experimentally, we have measured the rate of transport monitoring change in fluorescence intensity with time using the PAMPA method. Analysis of the experimental results showed that NAFA transport is substantially faster in POPC at pH 7.2 compared to DOPC at an identical pH. Whereas in a protonated environment, at pH 4.8, NAFA permeation becomes independent of membrane composition, producing transport rates that are almost identical in both DOPC and POPC. Computationally, we have conducted a wide variety of analyses to determine the effect of system size and lipid composition on the passive permeation of the phenylalanine dipeptide. This was undertaken in the broader context of exploring and explaining the passive permeation of aromatic amino acids through model cell membranes. In terms of the effect of system size, the potential of mean force was lowered slightly by about 3 kJ mol^{-1}, in a larger bilayer, potentially indicating that membrane fluctuations are not being well sampled with only 40 POPC lipids or indicating that a simulation length of 50 ns per window is insufficient to sample these fluctuations. A similar trend was also noticed for the mean first passage time, which is highly coupled with the results for the potential of mean force. Along these lines, it was more difficult to achieve convergence in the rotational sidechain anisotropy studies, even with simulations of 250 ns in length. A greater number of χ_1 and χ_2 sidechain conformations were observed in the interfacial region for POPC 50, indicating that the larger membrane system may accommodate more rarely sampled configurations. No difference was found in permeation coefficients, translational diffusion, insertion angles, Ramachandran plots, clustering, backbone oxygen-to-nitrogen distance, radius of gyration, solvent accessible surface area, radial distribution functions, and coordination numbers.

In terms of lipid composition, DOPC contains two, singly unsaturated acyl chains, and POPC has only a single unsaturated acyl chain. The addition of a double bond creates greater disorder within the lipid structure. This effect is most easily seen within the potential of mean force for DOPC where the PMF is broader than that for either of the POPC systems. This then affects the mean first passage time which is highly sensitive to changes in the PMF. The clustering and backbone oxygen-to-nitrogen distance analyses also indicate

that the DOPC system transitions to a C_{7eq} conformation sooner within the membrane. This also indicates a greater degree of disorder which allows the phenylalanine dipeptide to adopt this low energy conformation in more shallow regions of the lipid bilayer. No difference was observed in terms of permeation coefficients, translational diffusion, insertion angles, Ramachandran plots, radius of gyration, solvent accessible surface area, radial distribution functions, and coordination numbers.

Although only a few differences were present in terms of system size and lipid type, a wide variety of observations were made in terms of the general permeation process. The potential of mean force exhibited the typical pattern for amphiphilic molecules: an energy minimum near the interface and an energy maximum in the interior. Translational diffusion coefficients were largely unchanged with insertion depth, with a small decrease near the interfacial region. Accordingly, the mean first passage time closely followed the trend in terms of the potential of mean force at the center of the membrane. The computation of permeability coefficients was challenging due to variation with the choice of starting location within the aqueous simulation region. Sidechain rotation was more inhibited near the interfacial region and freer in either the aqueous or central membrane regions. In the permeation process, the sidechain enters the membrane first, then followed by the backbone, adduced by the insertion angle, radial distribution function, and coordination number analyses. Analysis of conformational dynamics indicates the presence of more freedom of movement within the aqueous region and more restricted conformational freedom within the center of the membrane. Overall, our studies have provided an experimental baseline and mechanistic interpretation for unassisted transport across lipid bilayers of a small di-peptide system.

Acknowledgements

GSJ would like to thank Dr. Richard A. Rivers for inspirational comments. GSJ would also like to acknowledge Dr. Eric M. González Morales of UCC for helpful suggestions. We would like acknowledge Center for Ressearch Computing resources at the University of Kansas.

Disclosure statement

No potential conflict of interest was reported by the author(s).

Funding

We would like to acknowledge the Center for Research Computing at the University of Kansas and on computer workstations supported by the General Research Fund at the University of Kansas. This project was supported in part by an NSF grant CHE1807852.

ORCID

Gouri S. Jas http://orcid.org/0000-0002-0774-012X

References

Allen, M. P., & Tildesley, D. J. (1989). *Computer simulation of liquids* (p. 385). Clarendon Press.

Awoonor-Williams, E., & Rowley, C. N. (2016). Molecular simulation of nonfacilitated membrane permeation. *Biochimica et Biophysica Acta*, *1858*(7 Pt B), 1672–1687. https://doi.org/10.1016/j.bbamem.2015.12.014

Bassolino-Klimas, D., Alper, H. E., & Stouch, T. R. (1993). Solute diffusion in lipid bilayer membranes: An atomic level study by molecular dynamics simulation. Biochemistry, *32*(47), 12624–12637. https://doi.org/10.1021/bi00210a010

Bassolino-Klimas, D., Alper, H. E., & Stouch, T. R. (1995). Mechanism of solute diffusion through lipid bilayer membranes by molecular dynamics simulation. *Journal of the American Chemical Society*, *117*(14), 4118–4129. https://doi.org/10.1021/ja00119a028

Bicout, D. J., & Szabo, A. (1998). Electron transfer reaction dynamics in non-Debye solvents. Journal *of Chemical Physics*, *109*(6), 2325–2338. https://doi.org/10.1063/1.476800

Bonhenry, D., Tarek, M., & Dehez, F. (2013). Effects of phospholipid composition on the transfer of a small cationic peptide across a model biological membrane. *Journal of Chemical Theory and Computation*, *9*(12), 5675–5684. https://doi.org/10.1021/ct400576e

Brooks, B. R., Brooks, C. L., Mackerell, A. D., Nilsson, L., Petrella, R. J., Roux, B., Won, Y., Archontis, G., Bartels, C., Boresch, S., Caflisch, A., Caves, L., Cui, Q., Dinner, A. R., Feig, M., Fischer, S., Gao, J., Hodoscek, M., Im, W., … Karplus, M. (2009). CHARMM: The biomolecular simulation program. *Journal of Computational Chemistry*, *30* (10), 1545–1614. https://doi.org/10.1002/jcc.21287

Bussi, G., Donadio, D., & Parrinello, M. (2007). Canonical sampling through velocity rescaling. *The Journal of Chemical Physics*, *126* (1), 14101. https://doi.org/10.1063/1.2408420

Cardenas, A. E., & Elber, R. (2013). Computational study of peptide permeation through membrane: Searching for hidden slow variables. *Molecular Physics*, *111*(22–23), 3565–3578. https://doi.org/10.1080/00268976.2013.842010

Cardenas, A. E., & Elber, R. (2014). Modeling kinetics and equilibrium of membranes with fields: Milestoning analysis and implication to permeation. *The Journal of Chemical Physics*, *141*(5), 54101. https://doi.org/10.1063/1.4891305

Cardenas, A. E., Jas, G. S., DeLeon, K. Y., Hegefeld, W. A., Kuczera, K., & Elber, R. (2012). Unassisted transport of N-Acetyl-L-tryptophanamide through membrane: Experiment and simulation of kinetics. *The Journal of Physical Chemistry. B*, *116*(9), 2739–2750. https://doi.org/10.1021/jp2102447

Carpenter, T. S., Kirshner, D. A., Lau, E. Y., Wong, S. E., Nilmeier, J. P., & Lightstone, F. C. (2014). A method to predict blood-brain barrier permeability of drug-like compounds using molecular dynamics simulations. *Biophysical Journal*, *107*(3), 630–641. https://doi.org/10.1016/j.bpj.2014.06.024

Cohen, B. E., & Bangham, A. D. (1972). Diffusion of small non-electrolytes across liposome membranes. Nature, *236*(5343), 173–174. https://doi.org/10.1038/236173a0

Comer, J., Phillips, J. C., Schulten, K., & Chipot, C. (2014). Multiple-replica strategies for free-energy calculations in NAMD: Multiple-walker adaptive biasing force and walker selection rules. *Journal of Chemical Theory and Computation*, *10*(12), 5276–5285. https://doi.org/10.1021/ct500874p

Comer, J., Schulten, K., & Chipot, C. (2014). Calculation of Lipid-bilayer permeabilities using an average force. *Journal of Chemical Theory and Computation*, *10*(2), 554–564. https://doi.org/10.1021/ct400925s

Corti, G., Maestrelli, F., Cirri, M., Zerrouk, N., & Mura, P. (2006). Development and evaluation of an in vitro method for prediction of human drug absorption II. Demonstration of the method suitability. *European Journal of Pharmaceutical Sciences: Official Journal of the European Federation for Pharmaceutical Sciences*, *27*(4), 354–362. https://doi.org/10.1016/j.ejps.2005.11.005

Di, L., Kerns, E. H., Fan, K., McConnell, O. J., & Carter, G. T. (2003). High throughput artificial membrane permeability assay for blood-brain

barrier. *European Journal of Medicinal Chemistry*, *38*(3), 223–232. https://doi.org/10.1016/s0223-5234(03)00012-6

Diamond, J. M., & Katz, Y. (1974). Interpretation of nonelectrolyte partition coefficients between dimyristoyl lecithin and water. *The Journal of Membrane Biology*, *17*(2), 121–154. https://doi.org/10.1007/BF01870176

Dobson, P. D., & Kell, D. B. (2008). Carrier-mediated cellular uptake of pharmaceutical drugs: An exception or the rule? *Nature Reviews. Drug Discovery*, *7*(3), 205–220. https://doi.org/10.1038/nrd2438

Dobson, P. D., Lanthaler, K., Oliver, S. G., & Kell, D. B. (2009). Implications of the dominant role of transporters in drug uptake by cells. *Current Topics in Medicinal Chemistry*, *9*(2), 163–181. https://doi.org/10.2174/156802609787521616

Faulkner, C., Santos-Carballal, D., Plant, D. F., & de Leeuw, N. H. (2020). Atomistic molecular dynamics simulations of propofol and fentanyl in phosphatidylcholine lipid bilayers. *ACS Omega*, *5*(24), 14340–14353. https://doi.org/10.1021/acsomega.0c00813

Fredriksson, R., Nordstrom, K. J., Stephansson, O., Hagglund, M. G., & Schioth, H. B. (2008). The solute carrier (SLC) complement of the human genome: Phylogenetic classification reveals four major families. *FEBS Letters*, *582*(27), 3811–3816. https://doi.org/10.1016/j.febslet.2008.10.016

Giacomini, K. M., Huang, S.-M., Tweedie, D. J., Benet, L. Z., Brouwer, K. L. R., Chu, X., Dahlin, A., Evers, R., Fischer, V., Hillgren, K. M., Hoffmaster, K. A., Ishikawa, T., Keppler, D., Kim, R. B., Lee, C. A., Niemi, M., Polli, J. W., Sugiyama, Y., Swaan, P. W., … Zhang, L. (2010). Membrane transporters in drug development. *Nature Reviews. Drug Discovery*, *9*(3), 215–236. https://doi.org/10.1038/nrd3028

Hogben, C. A., Tocco, D. J., Brodie, B. B., & Schanker, L. S. (1959). On the mechanism of intestinal absorption of drugs. *The Journal of Pharmacology and Experimental Therapeutics*, *125*(4), 275–282. PMID: 13642268

Högerle, M. L., & Winne, D. (1983). Drug absorption by the rat jejunum perfused in situ. Dissociation from the pH-partition theory and role of microclimate-pH and unstirred layer. *Naunyn-Schmiedeberg's Archives of Pharmacology*, *322*(4), 249–255. https://doi.org/10.1007/BF00508339

Hu, Y., Ou, S. C., & Patel, S. (2013). Free energetics of arginine permeation into model DMPC lipid bilayers: Coupling of effective counterion concentration and lateral bilayer dimensions. *The Journal of Physical Chemistry. B*, *117* (39), 11641–11653. https://doi.org/10.1021/jp404829y

Hummer, G. (2005). Position-dependent diffusion coefficients and free energies from Bayesian analysis of equilibrium and replica molecular dynamics simulations. *New Journal of Physics*, *7*(34), 34–14. https://doi.org/10.1088/1367-2630/7/1/034

Irvine, J. D., Takahashi, L., Lockhart, K., Cheong, J., Tolan, J. W., Selick, H. E., & Grove, J. R. (1999). MDCK (Madin-Darby canine kidney) cells: A tool for membrane permeability screening. *Journal of Pharmaceutical Sciences*, *88*(1), 28–33. https://doi.org/10.1021/js9803205

Jämbeck, J. P. M., & Lyubartsev, A. P. (2013). Exploring the free energy landscape of solutes embedded in lipid bilayers. *The Journal of Physical Chemistry Letters*, *4*(11), 1781–1787. https://doi.org/10.1021/jz4007993

Jo, S., Kim, T., & Im, W. (2007). Automated builder and database of protein/membrane complexes for molecular dynamics simulations. *PLoS One*, *2*(9), e880. https://doi.org/10.1371/journal.pone.0000880

Jo, S., Lim, J. B., Klauda, J. B., & Im, W. (2009). CHARMM-GUI membrane builder for mixed bilayers and its application to yeast membranes. *Biophysical Journal*, *97*(1), 50–58. https://doi.org/10.1016/j.bpj.2009.04.013

Jorgensen, W. L., Chandrasekhar, J., Madura, J. D., Impey, R. W., & Klein, M. L. (1983). Comparison of simple potential functions for simulating liquid water. Journal *of Chemical Physics*, *79*(2), 926–935. https://doi.org/10.1063/1.445869

Kansy, M., Senner, F., & Gubernator, K. (1998). Physicochemical high throughput screening: Parallel artificial membrane permeation assay in the description of passive absorption processes. *Journal of Medicinal Chemistry*, *41*(7), 1007–1010. https://doi.org/10.1021/jm970530e

Kästner, J. (2011). Umbrella sampling. *Wiley Interdisciplinary Reviews: Computational Molecular Science*, *1*(6), 932–942. https://doi.org/10.1002/wcms.66

Khuntawee, W., Wolschann, P., Rungrotmongkol, T., Wong-Ekkabut, J., & Hannongbua, S. (2015). Molecular dynamics simulations of the interaction of beta cyclodextrin with a lipid bilayer. *Journal of Chemical Information and Modeling*, *55*(9), 1894–1902. https://doi.org/10.1021/acs.jcim.5b00152

Klauda, J. B., Roberts, M. F., Redfield, A. G., Brooks, B. R., & Pastor, R. W. (2008). Rotation of lipids in membranes: Molecular dynamics simulation, ^{31}P spin-lattice relaxation, and rigid-body dynamics. *Biophysical Journal*, *94*(8), 3074–3083. https://doi.org/10.1529/biophysj.107.121806

Kuczera, K., Unruh, J., Johnson, C. K., & Jas, G. S. (2010). Reorientations of aromatic amino acids and their side chain models: Anisotropy measurements and molecular dynamics simulations. *The Journal of Physical Chemistry A*, *114*(1), 133–142. https://doi.org/10.1021/jp907382h

Kumar, S., Bouzida, D., Swendsen, R., Kollman, P., & Rosenberg, J. (1992). The weighted histogram analysis method for free-energy calculations on biomolecules.1. The method. *Journal of Computational Chemistry*, *13*(8), 1011–1021. https://doi.org/10.1002/jcc.540130812

Lee, B. L., & Kuczera, K. (2018). Simulating the free energy of passive membrane permeation for small molecules. Molecular *Simulation*, *44* (13–14), 1147–1157. https://doi.org/10.1080/08927022.2017.1407029

Lee, B. L., Kuczera, K., Middaugh, C. R., & Jas, G. S. (2016). Permeation of the three aromatic dipeptides through lipid bilayers: Experimental and computational study. *The Journal of Chemical Physics*, *144*(24), 245103. https://doi.org/10.1063/1.4954241

Leftin, A., Molugu, T. R., Job, C., Beyer, K., & Brown, M. F. (2014). Area per lipid and cholesterol interactions in membranes from separated local-field (13)C NMR spectroscopy. *Biophysical Journal*, *107*(10), 2274–2286. https://doi.org/10.1016/j.bpj.2014.07.044

Liu, Y., & Nagle, J. F. (2004). Diffuse scattering provides material parameters and electron density profiles of biomembranes. *Physical Review E*, *69*(4), 40901. https://doi.org/10.1103/PhysRevE.69.040901

Marrink, S.-J., & Berendsen, H. J. C. (1994). Simulation of water transport through a lipid membrane. *The Journal of Physical Chemistry*, *98*(15), 4155–4168. https://doi.org/10.1021/j100066a040

Marrink, S. J., & Berendsen, H. J. C. (1996). Permeation process of small molecules across lipid membranes studied by molecular dynamics simulations. *The Journal of Physical Chemistry*, *100* (41), 16729–16738. https://doi.org/10.1021/jp952956f

Meier, M., Blatter, X. L., Seelig, A., & Seelig, J. (2006). Interaction of verapamil with lipid membranes and P-glycoprotein: Connecting thermodynamics and membrane structure with functional activity. *Biophysical Journal*, *91*(8), 2943–2955. https://doi.org/10.1529/biophysj.106.089581

Mills, T. T., Toombes, G. E. S., Tristram-Nagle, S., Smilgies, D. M., Feigenson, G. W., & Nagle, J. F. (2008). Order parameters and areas in fluid-phase oriented lipid membranes using wide angle x-ray scattering. *Biophysical Journal*, *95*(2), 669–681. https://doi.org/10.1529/biophysj.107.127845

Neale, C., Bennett, W. F. D., Tieleman, D. P., & Pomes, R. (2011). Statistical convergence of equilibrium properties in simulations of molecular solutes embedded in lipid bilayers. *Journal of Chemical Theory and Computation*, *7* (12), 4175–4188. https://doi.org/10.1021/ct200316w

Nitschke, N., Atkovska, K., & Hub, J. S. (2016). Accelerating potential of mean force calculations for lipid membrane permeation: System size, reaction coordinate, solute-solute distance, and cutoffs. *The Journal of Chemical Physics*, *145* (12), 125101. https://doi.org/10.1063/1.4963192

Orsi, M., Sanderson, W. E., & Essex, J. W. (2009). Permeability of small molecules through a lipid bilayer: A multiscale simulation study. *The Journal of Physical Chemistry B*, *113*(35), 12019–12029. https://doi.org/10.1021/jp903248s

Parisio, G., Stocchero, M., & Ferrarini, A. (2013). Passive membrane permeability: Beyond the standard solubility-diffusion model. *Journal of Chemical Theory and Computation*, *9*(12), 5236–5246. https://doi.org/10.1021/ct400690t

Pastor, R. W., & MacKerell, A. D. (2011). Development of the CHARMM force field for lipids. *The Journal of Physical Chemistry Letters*, *2*(13), 1526–1532. https://doi.org/10.1021/jz200167q

Petersen, H. G. (1995). Accuracy and efficiency of the particle mesh Ewald method. Journal *of Chemical Physics*, *103*(9), 3668–3679. https://doi.org/10.1063/1.470043

Petrache, H. I., Tristram-Nagle, S., Gawrisch, K., Harries, D., Parsegian, V. A., & Nagle, J. F. (2004). Structure and fluctuations of charged phosphatidylserine bilayers in the absence of salt. *Biophysical Journal*, *86*(3), 1574–1586. https://doi.org/10.1016/S0006-3495(04)74225-3

Pronk, S., Pall, S., Schulz, R., Larsson, P., Bjelkmar, P., Apostolov, R., Shirts, M. R., Smith, J. C., Kasson, P. M., van der Spoel, D., Hess, B., & Lindahl, E. (2013). GROMACS 4.5: A high-throughput and highly parallel open source molecular simulation toolkit. *Bioinformatics (Oxford, England)*, *29*(7), 845–854. https://doi.org/10.1093/bioinformatics/btt055

Ramachandran, G., Ramakrishnan, C., & Sasisekharan, V. (1963). Stereochemistry of polypeptide chain configurations. *Journal of Molecular Biology*, *7*, 95–99. https://doi.org/10.1016/S0022-2836(63)80023-6

Roux, B. (1995). The calculation of the potential of mean force using computer-simulations. Computer *Physics Communications*, *91*(1–3), 275–282. https://doi.org/10.1016/0010-4655(95)00053-I

Schulten, K., Schulten, Z., & Szabo, A. (1981). Dynamics of reactions involving diffusive barrier crossing. Journal *of Chemical Physics*, *74*(8), 4426–4432. https://doi.org/10.1063/1.441684

Seelig, A. (2007). The role of size and charge for blood–brain barrier permeation of drugs and fatty acids. *Journal of Molecular Neuroscience*, *33*(1), 32–41. https://doi.org/10.1007/s12031-007-0055-y

Shinoda, W. (2016). Permeability across lipid membranes. *Biochimica et Biophysica Acta*, *1858*(10), 2254–2265. https://doi.org/10.1016/j.bbamem.2016.03.032

Snyder, R. G., Tu, K., Klein, M. L., Mendelssohn, R., Strauss, H. L., W., & Sun, W. (2002). Acyl chain conformation and packing in dipalmotoylphosphatidylcholine bilayers from MD simulation and IR spectroscopy. *The Journal of Physical Chemistry B*, *106*(24), 6273–6288. https://doi.org/10.1021/jp012145d

Souaille, M., & Roux, B. (2001). Extension to the weighted histogram analysis method: Combining umbrella sampling with free energy calculations. Computer *Physics Communications*, *135*(1), 40–57. https://doi.org/10.1016/S0010-4655(00)00215-0

Sugii, T., Takagi, S., & Matsumoto, Y. (2005). A molecular-dynamics study of lipid bilayers: Effects of the hydrocarbon chain length on permeability. *The Journal of Chemical Physics*, *123* (18), 184714. https://doi.org/10.1063/1.2102900

Tobias, D. J., & Brooks, C. L. (1992). Conformational equilibrium in the alanine dipeptide in the gas-phase and aqueous-solution - a comparison of theoretical results. *The Journal of Physical Chemistry*, *96*(9), 3864–3870. https://doi.org/10.1021/j100188a054

Torrie, G., & Valleau, J. (1977). Non-physical sampling distributions in Monte-Carlo free-energy estimation - Umbrella sampling. Journal *of Computational Physics*, *23*(2), 187–199. https://doi.org/10.1016/0021-9991(77)90121-8

Tu, K., Tobias, D. J., Blasie, J. K., & Klein, M. L. (1996). Molecular dynamics investigation of the structure of a fully hydrated gel phase dipalmitoylphosphatidylcholine bilayer. *Biophysical Journal*, *70*(2), 595–608. https://doi.org/10.1016/S0006-3495(96)79623-6

Ulander, J., & Haymet, A. D. J. (2003). Permeation across hydrated DPPC lipid bilayers: Simulation of the titrable amphiphilic drug valproic acid. *Biophysical Journal*, *85*(6), 3475–3484. https://doi.org/10.1016/S0006-3495(03)74768-7

Vanommeslaeghe, K., Hatcher, E., Acharya, C., Kundu, S., Zhong, S., Shim, J., Darian, E., Guvench, O., Lopes, P., Vorobyov, I., & Mackerell, A. D. (2010). CHARMM general force field: A force field for drug-like molecules compatible with the CHARMM all-atom additive biological force fields. *Journal of Computational Chemistry*, *31*(4), 671–690. https://doi.org/10.1002/jcc.21367

Vaz, W. L. C., & Almeida, P. F. (1991). Microscopic versus macroscopic diffusion in one-component fluid phase lipid bilayer membranes. *Biophysical Journal*, *60*(6), 1553–1554. https://doi.org/10.1016/S0006-3495(91)82190-7

Venable, R. M., Brooks, B. R., & Pastor, R. W. (2000). Molecular dynamics simulations of gel (LβI) phase lipid bilayers in constant and constant surface area ensembles. Journal *of Chemical Physics*, *112*(10), 4822–4832. https://doi.org/10.1063/1.481085

Wei, C., & Pohorille, A. (2014). Flip-flop of oleic acid in a phospholipid membrane: Rate and mechanism. *The Journal of Physical Chemistry B*, *118* (45), 12919–12926. https://doi.org/10.1021/jp508163e

Wohnsland, F., & Faller, B. (2001). High-throughput permeability pH profile and high-throughput alkane/water log P with artificial membranes. *Journal of Medicinal Chemistry*, *44*(6), 923–930. https://doi.org/10.1021/jm001020e

Wu, E. L., Cheng, X., Jo, S., Rui, H., Song, K. C., Dávila-Contreras, E. M., Qi, Y., Lee, J., Monje-Galvan, V., Venable, R. M., Klauda, J. B., & Im, W. (2014). CHARMM-GUI Membrane Builder toward realistic biological membrane simulations. *Journal of Computational Chemistry*, *35*(27), 1997–2004. https://doi.org/10.1002/jcc.23702

Xiang, T. X., & Anderson, B. D. (1998). Influence of chain ordering on the selectivity of dipalmitoyl phosphatidylcholine bilayer membranes for permeant size and shape. *Biophysical Journal*, *75*(6), 2658–2671. https://doi.org/10.1016/S0006-3495(98)77711-2

Xiang, T.-X., & Anderson, B. D. (2006). Liposomal drug transport: A molecular perspective from molecular dynamics simulations in lipid bilayers. *Advanced Drug Delivery Reviews*, *58*(12–13), 1357–1378. https://doi.org/10.1016/j.addr.2006.09.002

Zhu, C., Jiang, L., Chen, T. M., & Hwang, K. K. (2002). A comparative study of artificial membrane permeability assay for high throughput profiling of drug absorption potential. *European Journal of Medicinal Chemistry*, *37*(5), 399–407. https://doi.org/10.1016/S0223-5234(02)01360-0

Zusman, L. D. (1980). Outer-sphere electron-transfer in polar-solvents. *Chemical Physics*, *49*(2), 295–304. https://doi.org/10.1016/0301-0104(80)85267-0